Self-healing Materials

Fundamentals, Design Strategies, and Applications

Edited by
Swapan Kumar Ghosh

WILEY-VCH Verlag GmbH & Co. KGaA

Contents

Preface

Scientists have altered the properties of materials such as metals, alloys, polymers, and so on, to suit the ever changing needs of our society. As we entered into the twenty-first century, search of advanced materials with crack avoidance and long-term durability is on high priority. The challenge for material scientists is therefore to develop new technologies that can produce novel materials with increased safety, extended lifetime and no aftercare or a very less amount of repairing costs. To stimulate this interdisciplinary research in materials technology, the idea of compiling a book came to my mind in 2005. When I contacted one of the pioneer scientists in this field he remarked that it is too early to write a book on such a topic. His opinion was right because the field of material science and technology is rapidly advancing and it would be worth to wait few more years to include the latest updates. Thus this book is complied when the field of self-healing materials research is not matured enough as it is in its childhood.

The title Self-healing Materials itself describes the context of this book. It intends to provide its readers an upto date introduction of the field of self-healing materials (broadly divided into four classes—metals, polymers, ceramics/concretes, and coatings) with the emphasis on synthesis, structure, property, and possible applications. Though this book is mainly devoted to the scientists and engineers in industry and academia as its principle audience, it can also be recommended for graduate courses.

This book with its nine chapters written by international experts gives a wide coverage of many rapidly advancing fields of material science and engineering. The introductory chapter addresses the definition, broad spectrum of strategies, and application potentials of self-healing materials. Chapter 2 summarizes the recent advances in crack healing of polymers and polymer composites. Self-healing in most common polymeric structures occurs through chemical reactions. However, in the case of ionic polymers or ionomers healing follows a different mechanism. This is the subject of Chapter 3. Corrosion causes severe damages to metals. Encapsulated corrosion inhibitors can be incorporated into coatings to provide self-healing capabilities in corrosion prevention of metallic substrates. This is dealt in Chapter 4. Ceramics are emerging as key materials for structural applications. Chapter 5 describes the self-healing capability of ceramic materials. Concrete is the

Self-healing Materials: Fundamentals, Design Strategies, and Applications. Edited by Swapan Kumar Ghosh

ISBN: 978-3-527-31829-2

most widely used man made materials for structural applications. The possibility of introducing self-healing function in cements is the key subject of Chapter 6. Self-healing in metals is dealt in Chapter 7 while its subsequent Chapter 8 provides an insight of self-healing phenomenon in metallic alloys. The last chapter of this book describes the developments of a model to predict the effects of distributed damages and its subsequent self-healing processes in fiber reinforced polymer composites.

I hope the above mentioned chapters will deliver the readers useful information on self-healing material developments. I am grateful to the contributing authors of this book for their assistance to make this project a success. I would also like to thank the whole Wiley-VCH team involved in this project. Though, last but not least, I would like to dedicate this book to my wife Anjana and son Subhojit for their constant support and encouragement in this venture.

Swapan Kumar Ghosh
September 2008

List of Contributors

Kotoji Ando
Yokohama National University
Department of Energy & Safety Engineering
79-5, Tokiwadai, Hodogaya-ku
Yokohama 240-8501
Japan

Ever J. Barbero
West Virginia University
Mechanical and Aerospace Engineering
Morgantown, WV 26506-6106
USA

Kevin J. Ford
West Virginia University
Mechanical and Aerospace Engineering
Morgantown, WV 26506-6106
USA

Christopher Joseph
Cardiff School of Engineering
Queen's Buildings
The Parade
Newport Road
Cardiff CF24 3AA
United Kingdom

Stephen James Kalista, Jr.
Washington and Lee University
Department of Physics and Engineering
204 West Washington Street
Lexington, VA 24450
USA

Swapan Kumar Ghosh
ProCoat India Private Limited
Kalayaninagar, Pune-411 014
India

Michele V. Manuel
University of Florida
Department of Materials Science and Engineering
152 Rhines Hall
P.O. Box 116400
Gainesville, FL 32611-6400
USA

Joan A. Mayugo
Escola Politècnica Superior
University de Girona
Campus Montilvi, 17071 Girona
Spain

Wataru Nakao
Yokohama National University
Interdisciplinary Research Center
79-5, Tokiwadai, Hodogaya-ku,
Yokohama, 240-8501,
Japan

Min Zhi Rong
Materials Science Institute
Zhongshan University
135# Xin-Gang-Xi Rd.
Guangzhou 510275
P. R. China

Self-healing Materials: Fundamentals, Design Strategies, and Applications. Edited by Swapan Kumar Ghosh

ISBN: 978-3-527-31829-2

Erik Schlangen
Delft University of Technology
Department of Civil Engineering and Geosciences
P.O. Box 5048
2600 GA Delft
The Netherlands

Norio Shinya
Innovative Materials Engineering Laboratory,
Sengen Site,
National Institute for Materials Science
1-2-1, Sengen,
Tsukuba, Ibaraki 305-0047
Japan

Koji Takahashi
Yokohama National University
Division of Materials Science and Engineering
79-5, Tokiwadai, Hodogaya-ku
Yokohama, 240-8501
Japan

Tao Yin
Materials Science Institute
Zhongshan University
135# Xin-Gang-Xi Rd.
Guangzhou 510275
P. R. China

Ming Qiu Zhang
Materials Science Institute
Zhongshan University
135# Xin-Gang-Xi Rd.
Guangzhou 510275
P. R. China

Mikhail Zheludkevich
Department of Ceramics and Glass Engineering, CICECO, University of Aveiro,
Campus Universitario de Santiago,
3810-193
Aveiro
Portugal

9
Modeling Self-healing of Fiber-reinforced Polymer–matrix Composites with Distributed Damage

Ever J. Barbero, Kevin J. Ford and Joan A. Mayugo

9.1
Introduction

Composite materials are formed by the combination of two or more distinct materials to form a new material with enhanced properties [1]. Recently, self-healing polymers and composites have been proposed. One system in particular incorporates the use of ruthenium catalyst and urea-formaldehyde microcapsules filled with dicyclopentadiene (DCPD) [2]. Barbero and Ford [3] accomplished self-healing of glass fiber-reinforced epoxy laminates by intralaminar dispersion of healing agent and catalyst. The healing agent, DCPD, is encapsulated and then dispersed in the epoxy resin during hand layup. The catalyst is also encapsulated and dispersed in a similar manner. Vacuum bagging technique is used to consolidate the samples that are cured at room temperature. Then, experiments are performed to reveal damage, plasticity, and healing of laminates under cyclic load.

Barbero *et al.* [4] developed a continuous damage and healing mechanics (CDHM) model to predict the effects of damage and subsequent self-healing as a function of load history. In Ref [4], damage and healing are represented in separate thermodynamic spaces. The damage portion of the model has been extensively identified and verified with data available in the literature [5, Chapter 8]. The self-healing portion of the previous model could not be identified or verified because of lack of experimental data for laminates undergoing distributed damage (e.g. microcracking). Until recently, data existed only for fracture toughness recovery due to healing of macrocracks [2, 6–8]. Then, Barbero and Ford [3] conducted a comprehensive experimental study to identify the healing portion of the model. Their experimental evidence suggests that simplification of the earlier model is possible, thus motivating the model presented in this chapter. Specifically, a damage/healing model where both effects are described in a single thermodynamic space is presented, thus simplifying considerably the earlier model.

The continuum damage-healing mechanics model proposed herein consists of a continuum damage mechanics model extended to account for healing effects. The model must be identified with experimental data from unidirectional or cross-ply laminates. Therefore, a methodology for identification of the damage and healing parameters of the model is described. Once identified, the model is capable of predicting damage and healing evolution of other laminate stacking sequence (LSS). Prediction of damage, healing, damage hardening, and hardening recovery upon healing are accomplished.

The model presented herein is likely to work, with modifications, for other healing processes such as geological rock densification [9], self-healing of concrete [10, 11], self-healing of ceramic materials [12, 13], bone remodeling, wounded skin regeneration [14–16], and compaction of crushed rock salt [9].

9.2 Damage Model

In this chapter, damage is represented by its effects on residual stiffness and strength. No attempt is made to identify actual microstructural modes of damage. However, various components of the model, namely, the damage variable adopted and several simplifying assumptions are rooted in experimental evidence. The model is composed of three main ingredients, the damage variable, the free-energy potential, and the damage evolution equations.

9.2.1 Damage Variable

Damage represents distributed, irreversible phenomena that cause stiffness and strength reductions. The choice of damage variable has a direct impact on the number of material parameters required to describe the phenomena and the accuracy of the model predictions. In this work, damage is represented by a second-order tensor $\mathbf{D}$. For convenience, the integrity tensor is defined as $\boldsymbol{\Omega} = \sqrt{\mathbf{I} - \mathbf{D}}$, where $\mathbf{I}$ is the second-order identity tensor.

Experimental evidence suggests that damage in the form of microcracks, delamination, fiber break, and so on, occur in planes parallel to the principal material directions. Therefore, it is assumed that the principal directions of damage n_1, n_2, n_3 coincide with the material orientations x_1, x_2, x_3. In this case, the damage tensor can be described by its three eigenvalues d_1, d_2, d_3. Such simplification allows us to think of the eigenvalues as a representation of fictitious, equivalent system of cracks that represent damage in the longitudinal, transverse, and thickness directions, respectively.

The model is developed taking two configurations into account: damaged and effective. In the damaged (actual) configuration, the material is subjected to nominal stress and undergoes damage $\mathbb{D}$, which results in reduced stiffness $\mathbb{C}(\mathbb{D})$. The effective configuration is a fictitious configuration where an increased effective

stress $\overline{\boldsymbol{\sigma}}$ acts upon a fictitious material having undamaged (virgin) elastic stiffness $\overline{\mathbf{C}}$. According to the energy equivalence hypothesis ([5, Chapter 8]), the elastic energy in the actual and effective configurations is identical.

The transformation of stress and strain between effective and damaged configurations is accomplished by

$$\overline{\sigma}_{ij} = M^{-1}_{ijkl}\sigma_{kl}; \quad \overline{\varepsilon}^e_{ij} = M_{ijkl}\varepsilon^e_{kl} \tag{9.1}$$

where an over-bar indicates that the quantity is evaluated in the effective configuration, the superscript e denotes quantities in the elastic domain, and $\mathbf{M}$ is the *damage effect tensor* defined as

$$M_{ijkl} = \frac{1}{2}(\Omega_{ik}\Omega_{jl} + \Omega_{il}\Omega_{jk}) \tag{9.2}$$

The stress–strain relationship in the effective configuration is simply that of a linearly elastic material with virgin properties, given by

$$\overline{\sigma}_{ij} = \overline{C}_{ijkl}\overline{\varepsilon}^e_{kl}; \quad \overline{\varepsilon}^e_{ij} = \overline{C}^{-1}_{ijkl}\overline{\sigma}_{kl} = \overline{S}_{ijkl}\overline{\sigma}_{kl} \tag{9.3}$$

The constitutive equation in the damaged configuration is obtained by substituting Equations 9.3 into Equations 9.1,

$$\begin{aligned}
&\sigma_{ij} = M_{ijkl}\overline{\sigma}_{kl} = M_{ijkl}\overline{C}_{klrs}\overline{\varepsilon}^e_{rs}, && \varepsilon^e_{ij} = M^{-1}_{ijkl}\overline{\varepsilon}^e_{kl} = M^{-1}_{ijkl}\overline{S}_{klrs}\overline{\sigma}_{rs},\\
&\sigma_{ij} = M_{ijkl}\overline{C}_{klrs}M_{rstu}\varepsilon^e_{tu}, && \varepsilon^e_{ij} = M^{-1}_{ijkl}\overline{S}_{klrs}M^{-1}_{ijkl}\sigma_{tu},\\
&\sigma_{ij} = C_{ijkl}\varepsilon^e_{kl}, && \varepsilon^e_{ij} = S_{ijkl}\sigma_{kl}
\end{aligned} \tag{9.4}$$

where by virtue of $\mathbf{M}$ being symmetric and using the energy equivalence hypothesis, the constitutive tensors $\mathbf{C}$ and $\mathbf{S}$ in the damaged domain are symmetric tensors given by

$$C_{ijkl} = M_{ijkl}\overline{C}_{klrs}M_{rstu}; \quad S_{ijkl} = M^{-1}_{ijkl}\overline{S}_{klrs}M^{-1}_{rstu} \tag{9.5}$$

9.2.2 Free-energy Potential

The constitutive equations are derived from thermodynamic principles. The Helmholtz free energy includes the elastic energy and additional terms to represent the evolution of the internal parameters as follows:

$$\psi = \varphi(\boldsymbol{\varepsilon}, \boldsymbol{\varepsilon}^{\mathrm{p}}, D) - c^d_1\left[c^d_2 \exp\left(\frac{\delta}{c^d_2}\right)\right] - c^p_1\left[c^p_2 \exp\left(\frac{\delta}{c^p_2}\right)\right] \tag{9.6}$$

where $\boldsymbol{\varepsilon}$, $\boldsymbol{\varepsilon}^{\mathrm{p}}$ are the elastic and plastic strain tensors, respectively; p, δ are the hardening variables, and $c^d_1, c^d_2, c^p_1, c^p_2$, are material parameters used to adjust the model to experimental data.

The following thermodynamic state laws can be obtained by satisfying the Clausius–Duhem inequality [17], thus assuring nonnegative dissipation

$$\boldsymbol{\sigma}_{ij} = \frac{\partial \psi}{\partial \varepsilon^e_{ij}} = C_{ijkl}(\varepsilon_{kl} - \varepsilon^p_{kl}) = C_{ijkl}\varepsilon^e_{kl} \tag{9.7}$$

$$Y_{ij} = -\frac{\partial \psi}{\partial D_{ij}} = -\frac{1}{2}(\varepsilon_{kl} - \varepsilon^p_{kl})\frac{\partial C_{klpq}}{\partial D_{ij}}(\varepsilon_{pq} - \varepsilon^p_{pq}) = -\frac{1}{2}\varepsilon^e_{kl}\frac{\partial C_{klpq}}{\partial D_{ij}}\varepsilon^e_{pq} \tag{9.8}$$

$$\gamma(\delta) = -\frac{\partial \psi}{\partial \delta} = c^d_1\left[\exp\left(\frac{\delta}{c^d_2}\right) - 1\right] \tag{9.9}$$

$$R(p) = -\frac{\partial \psi}{\partial p} = c^p_1\left[\exp\left(\frac{p}{c^p_2}\right) - 1\right] \tag{9.10}$$

where σ, $\mathbf{Y}$, γ, and R are the thermodynamic forces associated with the internal state variables ε, $\mathbf{D}$, p, and δ.

The thermodynamic forces can be written explicitly in terms of stress [5, Appendix 2] as

$$\begin{aligned}
Y_{11} &= \frac{1}{\Omega_1^2}\left(\frac{\overline{S}_{11}}{\Omega_1^4}\sigma_1^2 + \frac{\overline{S}_{12}}{\Omega_1^2\Omega_2^2}\sigma_2\sigma_1 + \frac{\overline{S}_{13}}{\Omega_1^2\Omega_3^2}\sigma_3\sigma_1 + \frac{2\overline{S}_{55}}{\Omega_1^2\Omega_3^2}\sigma_5^2 + \frac{2\overline{S}_{66}}{\Omega_1^2\Omega_2^2}\sigma_6^2\right)\\
Y_{22} &= \frac{1}{\Omega_2^2}\left(\frac{\overline{S}_{22}}{\Omega_2^4}\sigma_2^2 + \frac{\overline{S}_{12}}{\Omega_2^2\Omega_1^2}\sigma_2\sigma_1 + \frac{\overline{S}_{23}}{\Omega_2^2\Omega_3^2}\sigma_3\sigma_2 + \frac{2\overline{S}_{44}}{\Omega_2^2\Omega_3^2}\sigma_4^2 + \frac{2\overline{S}_{66}}{\Omega_2^2\Omega_1^2}\sigma_6^2\right)\\
Y_{33} &= \frac{1}{\Omega_3^2}\left(\frac{\overline{S}_{33}}{\Omega_3^4}\sigma_3^2 + \frac{\overline{S}_{13}}{\Omega_3^2\Omega_1^2}\sigma_3\sigma_1 + \frac{\overline{S}_{23}}{\Omega_3^2\Omega_2^2}\sigma_3\sigma_2 + \frac{2\overline{S}_{44}}{\Omega_3^2\Omega_2^2}\sigma_4^2 + \frac{2\overline{S}_{55}}{\Omega_3^2\Omega_1^2}\sigma_5^2\right)
\end{aligned} \tag{9.11}$$

9.2.3 Damage Evolution Equations

The evolution of the internal variables is defined as follows. First, damage initiation is controlled by a damage function, such as

$$g^d = \sqrt{\widehat{Y}^N : J : \widehat{Y}^N} + \sqrt{\widehat{Y}^S : B : \widehat{Y}^S} - [\gamma(\delta) + \gamma_0] \tag{9.12}$$

where γ_0 is the damage threshold and defines the hardening function. For plane stress, and taking into account the symmetry of the thermodynamic force tensor $\mathbf{Y}$, the damage surface is given by Equation 9.12 with parameters A_1, A_2, B_1, B_2, J_1, J_2.

The thermodynamic force tensor is assumed to be separable into a component $\mathbf{Y^N}$ arising from normal strains and a component $\mathbf{Y^S} = \mathbf{Y} - \mathbf{Y^N}$ arising from shear strains

$$\widehat{Y}^N = \widehat{A} : Y^N$$

$$\widehat{A}_{ijkl} = I_{ijkl} + (A_m - 1)\delta_{im}\delta_{jm}\delta_{km}\delta_{lm}\frac{\left(1 - \frac{\varepsilon_m}{|\varepsilon_m|}\right)}{2} \tag{9.13}$$

with $m = 1, 2, 3$. The values of ϵ_m are the values of the three normal strains in the principal material directions. The three values A_m represent the relation between damage thresholds in uniaxial compression and uniaxial extension in the principal material directions. The coefficients in the diagonal, fourth order, positive definite tensors **A**, **B**, **J** are calculated from available experimental data for unidirectional or cross-ply laminates as explained in Ref. [5, Chapter 9], while the parameters are determined by using experimental in-plane shear stress–strain data.

On the other hand, the plastic strain evolution is modeled by classical plasticity formulation [5, Chapter 9] and an associate flow rule. For the yield surface, a three-dimensional Tsai–Wu criterion shape is chosen due to its ability to represent different behavior among the different load paths in stress space. Plastic strains and damage effects are coupled by formulating the plasticity model in effective stress space. Therefore, the yield surface is a function of the thermodynamic forces $\overline{\sigma}$, R in the effective configuration as follows:

$$g^p = \sqrt{f_{ij}\overline{\sigma}_i\overline{\sigma}_j + f_i\overline{\sigma}_j} - [R(p) + R_0] \tag{9.14}$$

where $i = 1, 2, 6$, R_0 is the yield stress, and R is defined by the hardening law. The coefficients f_i, f_{ij} are obtained from the strength properties of unidirectional or cross-ply laminates in terms of the lamina strength values as follows:

$$\begin{aligned}
f_1 &= \frac{1}{\overline{F}_{1t}} - \frac{1}{\overline{F}_{1c}}; & f_2 &= \frac{1}{\overline{F}_{2t}} - \frac{1}{\overline{F}_{2c}}; & f_3 &= \frac{1}{\overline{F}_{3t}} - \frac{1}{\overline{F}_{3c}};\\
f_{11} &= \frac{1}{\overline{F}_{1t}\overline{F}_{1c}}; & f_{22} &= \frac{1}{\overline{F}_{2t}\overline{F}_{2c}}; & f_{33} &= \frac{1}{\overline{F}_{3t}\overline{F}_{3c}};\\
f_{44} &= \frac{1}{\overline{F}_4^2}; & f_{55} &= \frac{1}{\overline{F}_5^2}; & f_{66} &= \frac{1}{\overline{F}_6^2};\\
f_{23} &\cong -\frac{1}{2}(f_{22}f_{33})^{1/2}; & f_{13} &\cong -\frac{1}{2}(f_{11}f_{33})^{1/2}; & f_{12} &\cong -\frac{1}{2}(f_{11}f_{22})^{1/2}
\end{aligned} \tag{9.15}$$

The parameters F_{it}, F_{ic}, and F_i are the effective strength values. That is, the strength values in effective configuration. They are defined as

$$\begin{aligned}
\overline{F}_{1t} &= \frac{F_{1t}}{\Omega_{1t}}; & \overline{F}_{2t} &= \frac{F_{2t}}{\Omega_{2t}}; & \overline{F}_{3t} &= \frac{F_{3t}}{\Omega_{3t}};\\
\overline{F}_{1c} &= \frac{F_{1c}}{\Omega_{1c}}; & \overline{F}_{2c} &= \frac{F_{2c}}{\Omega_{2c}}; & \overline{F}_{3c} &= \frac{F_{3c}}{\Omega_{3c}};\\
\overline{F}_4 &= F_4\frac{\overline{G}_{12}}{G^*_{12}}\frac{\overline{G}_{13}}{G^*_{13}}; & \overline{F}_5 &= F_5\frac{\overline{G}_{13}}{G^*_{13}}; & \overline{F}_6 &= F_6\frac{\overline{G}_{12}}{G^*_{12}}
\end{aligned} \tag{9.16}$$

where the parameters F_{it} and F_{ic} (with $i = 1, 2, 3$), and F_i (with $i = 4, 5, 6$) are the strength values in tension, compression, in-plane shear, and out-of-plane shear for a composite lamina. G_i^* and G_i (with $i = 12, 13$) are the damaged shear modulus and the undamaged shear modulus, respectively. These values are tabulated in the literature or they can be easily obtained following standardized test methods [3, 18].

The evolution of internal variables is defined by flow rules

$$\dot{\bar{\varepsilon}}^p_{ij} = \dot{\lambda}^p \frac{\partial g^p}{\partial \bar{\sigma}_{ij}}; \quad \dot{p} = \dot{\lambda}^p \frac{\partial g^p}{\partial R}$$
$$\dot{D}_{ij} = \dot{\lambda}^d \frac{\partial g^d}{\partial Y_{ij}}; \quad \dot{\delta} = \dot{\lambda}^d \frac{\partial g^d}{\partial \gamma} \tag{9.17}$$

in terms of plastic strain and damage multipliers $\dot{\lambda}^p$, $\dot{\lambda}^d$. These are found by using a return mapping algorithm [5, Chapter 9].

9.3 Healing Model

Healing represents the extent of repair of distributed damage. Similar to damage, healing is represented by second-order tensor **H**. Since healing can only heal existing damage, healing is represented by a diagonal tensor with principal directions aligned with those of the damage tensor **D**. The principal values h_1, h_2, h_3 represent the area recovery normal to the principal directions, which are aligned with the material directions x_1, x_2, x_3 in the material coordinate system. As a consequence of the particular definition of damage and healing used herein, the healing model presented uses the same thermodynamic space for damage and healing. That is, both damage and healing are defined in the space of thermodynamic damage forces **Y**.

In Refs [7, 19], the crack-healing efficiency is defined as the percentage recovery of fracture toughness measured by tapered double cantilever beam (TDCB). In this chapter, it is postulated that the healing tensor is proportional to the damage tensor

$$h_i = \eta_i d_i \tag{9.18}$$

The proportionality constant is the efficiency of the healing system. Furthermore, healing represents recovery of damage. Therefore, the principal values of the healed–damage tensor are given by

$$d^h_i = d_i - h_i = d_i(1 - \eta) \tag{9.19}$$

Experimentally, it is possible to measure the following (Figure 9.1):

- the virgin moduli $\bar{G}_i$ from the initial slope of the first cycle of loading;
- the damaged moduli $G_i{}^d$ from the unloading portion of the first cycle; and
- the healed moduli G^h_i from the loading portion of the second cycle (after healing).

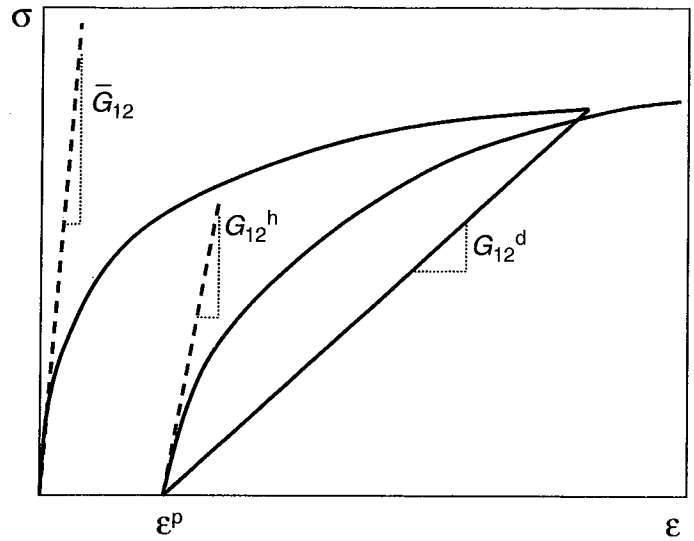

Fig. 9.1 Definition of measurable, relevant variables.

From these data, the efficiency is defined here as

$$\eta_i = \frac{G_i^h - G_i^d}{\bar{G}_i - G_i^d} \tag{9.20}$$

For composites reinforced by strong fibers, the self-healing system is incapable of healing fiber damage, which results in $\eta_1 = 0$. Once the self-healing polymer is released, it travels by capillary action and penetrates all the microcracks regardless of orientation, and thus $\eta_2 = \eta_3 = \eta$.

Once the material damages, higher levels of thermodynamic damage force $\mathbf{Y}$ are required to produce more damage. Higher thermodynamic damage force requires higher stress and correspondingly higher applied strain. This process, which is called *damage hardening*, is represented in the model by a state variable, the hardening parameter δ, which is a monotonically increasing function that provides a threshold below which no further damage can occur. A secondary effect of healing is to reduce the hardening threshold. That is, after healing, further damage can occur below the previous damage hardening threshold because some of the damage has been repaired. The model proposed herein captures this behavior by the following reduction in the damage hardening parameter

$$\delta^h = \delta(1 - \eta) \tag{9.21}$$

When the material is completely repaired, one has $\eta = 1$, $\delta = 0$, $\gamma = 0$ in the hardening law and the threshold for damage returns to the value for the virgin material. Thus, the material will begin to damage at the same threshold load as that of the virgin material. When the healing agent is exhausted, $\eta = 0$ and the material is just a damaging material with $\delta^h = \delta$; $\gamma \neq 0$ in the damage hardening

law, while the threshold for damage continues to increase, thus representing the normal hardening behavior of a purely damaging material.

9.4 Damage and Plasticity Identification

For damage without healing, the damage parameters are A_1, A_2, B_1, B_2, J_1, J_2, γ_0, c_1^d, c_2^d. Plasticity entails additional parameters as follows: f_i, f_{ij}, R_0, c_1^p, c_2^p. All these parameters depend on the following material properties, which are experimentally determined using standard testing methods:

- stiffness values (E_1, E_2, G_{12})
- strength values (F_{1t}, F_{1c}, F_{2c}, F_{2t}, F_6)
- critical damage values (d_{1t}, d_{1c}, d_{2t})
- damaged shear moduli at imminent failure (G_{12}^*)
- in-plane shear plastic threshold (F_6^{EP})
- in-plane shear damage threshold (F_6^{ED})
- plastic strain (γ_6^p) as a function of total applied strain (γ_6)

Cyclic shear stress–strain tests are used to obtain the nonlinear damaging behavior $\sigma_6(\gamma_6)$, as shown in Figure 9.2. The loading modulus is measured within a range of strain specified by the standard. The unloading modulus is measured over the entire unloading portion of the data.

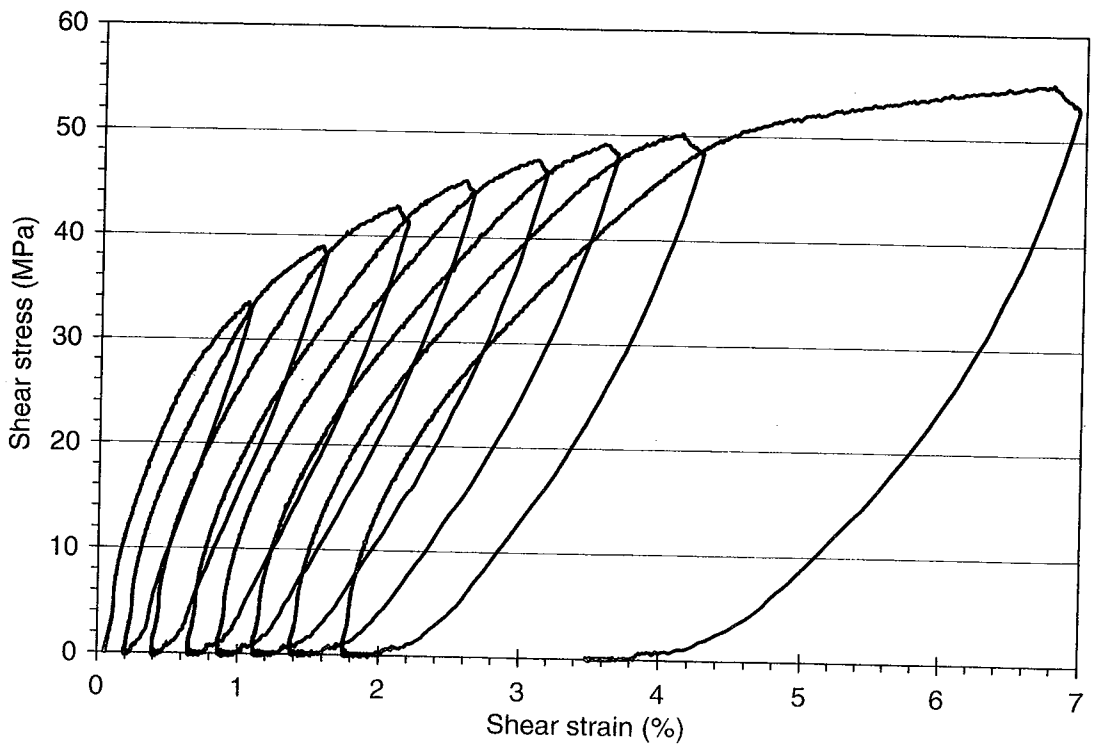

Fig. 9.2 Shear stress–strain behavior of unidirectional, neat specimen (no self-healing system). Loss of stiffness and accumulation of plastic strain are evident [3].

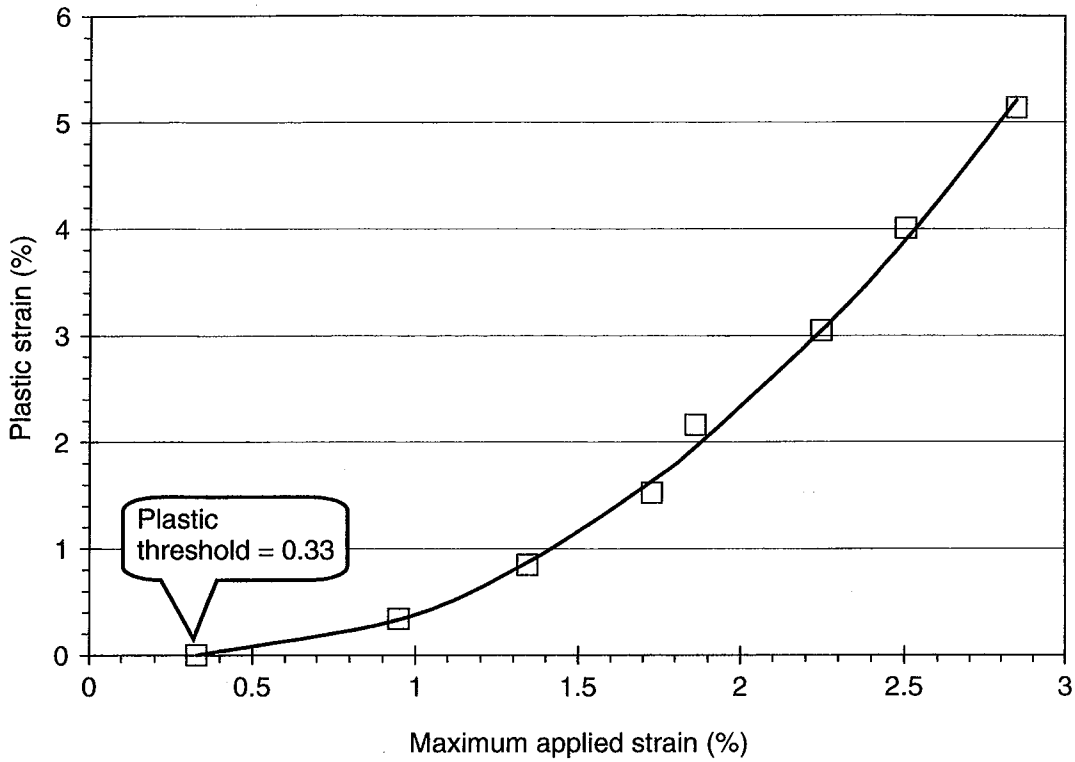

Fig. 9.3 Plastic strain versus applied strain for unidirectional, neat specimen (no self-healing system). Threshold plastic strain (i.e. yield strain) is evident [3].

Unrecoverable (plastic) strain can be observed upon unloading, but only after a threshold value of stress (i.e. the yield strength) or strain (i.e. the yield strain) is reached during loading (Figure 9.3).

Even though plastic strain is accumulated, initially the unloading modulus remains unchanged and equal to the loading modulus. For the unloading modulus to change, that is, to decrease below the value of the initial loading modulus, damage must appear. Note that the word "unloading" is added for emphasis and because the reduction in modulus is first detected during unloading of the specimen. But, of course, the modulus reduction is permanent. A reduction in the unloading modulus with respect to the initial loading modulus can be observed only after a threshold value of stress (i.e. the damage threshold stress) or strain (i.e. the damage threshold strain) is reached during loading (Figure 9.4).

The threshold stress F_{6EP} for appearance of unrecoverable (plastic) strain (i.e. the yield strength) and the threshold stress F_{6ED} for appearance of irreversible damage are read from the loading portion of the $\sigma_6(\gamma_6)$ curve (Figure 9.2) with the aid of Figures 9.3 and 9.4 (see also [5, chapter 9]). The unrecoverable (plastic) strain γ_6^p as a function of the applied total strain γ_6 is read for each cycle after full unloading and reported in Figure 9.3. The slope of the unloading curves provides the damaged elastic modulus G_{12}^d as a function of total applied strain γ_6 (Figure 9.4).

Existence of damage and a damage threshold are demonstrated by the fact that measured unloading modulus is less than the loading modulus after the damage threshold has been reached (Figure 9.4). No loss of stiffness occurs when the

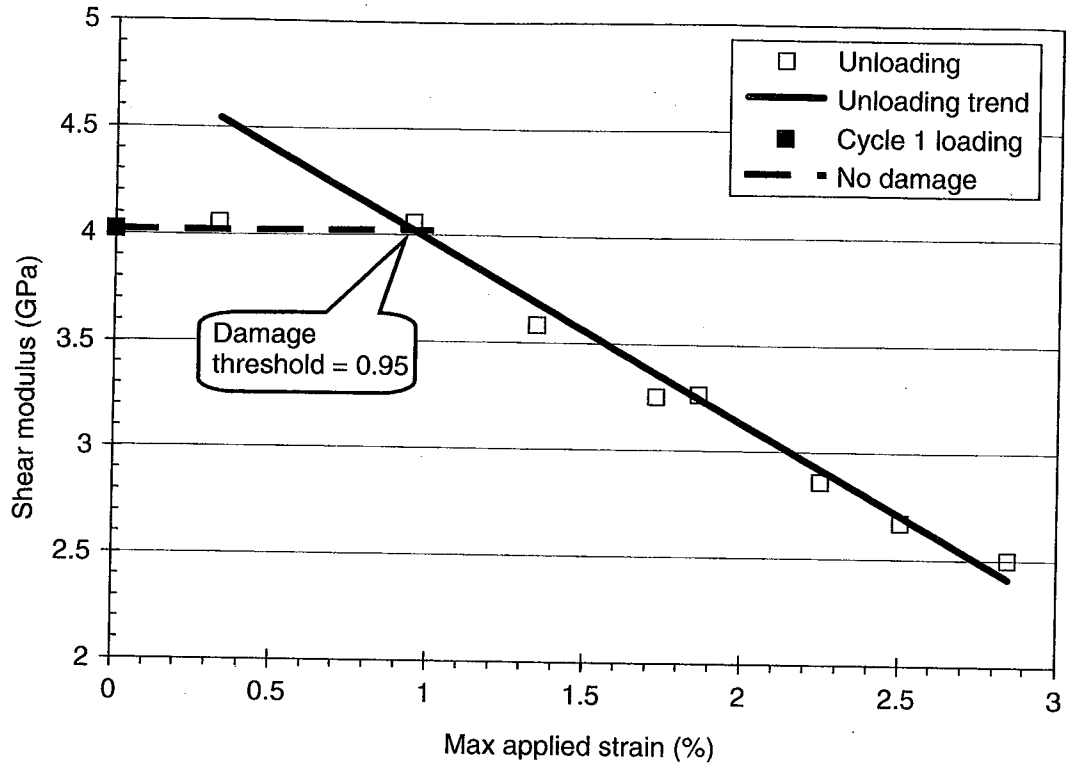

Fig. 9.4 Shear modulus versus applied strain of unidirectional, neat specimen (no self-healing system). Threshold damage strain is evident [3].

applied strain is less than the threshold. After the threshold is reached, the loss of modulus is proportional to the applied strain. Since careful visual inspection after each loading cycle does not reveal appearance of any macrocrack, the loss of modulus is attributed and modeled as distributed damage.

Also noticeable in Figure 9.3 is the accumulation of unrecoverable (plastic) strain. Although the physical, microstructural, and morphological mechanisms leading to plasticity in polymers are different than those leading to plasticity in metals, from a phenomenological and modeling point of view, unrecoverable deformations can be modeled with plasticity theory as long as the plastic strains are not associated to a reduction in the unloading modulus. The reduction in unloading modulus, which occurs independent of the plastic strain, can be accounted for by continuum damage mechanics. Each of these two phenomena has different thresholds for initiation and evolve with different rates. They are, however, coupled by the redistribution of stress that both phenomena induce. In the model, this is taken into account by formulating the plasticity model in terms of effective stress computed by the damage model [4].

Shear tests reveal marked nonlinearity (Figure 9.2) reaching almost total loss of tangent stiffness prior to failure, which occurs at large values of shear strain. Unloading secant stiffness reveals marked loss of stiffness due to damage, which worsens during cyclic reloading (Figure 9.4). Also, unloading reveals significant plastic strains accumulating during cyclic reloading (Figure 9.3).

The standard test method ASTM-D-3039 is used to determine E_1, E_2, ν_{12}, F_{1t}, F_{2t}. The standard test method SACMA-SRM-1R-94 is used to determine F_{1c}, F_{2c}. The standard test method ASTM-D-5379 is used to determine G_{12}, F_6. The configuration of ASTM-D-5379 is used to determine G_{12} as a function of damage, healing, and number of cycles. Also γ_6^p, F_6^{EP}, F_6^{ED} are found using the same test configuration. The identification procedure linking the damage and plasticity parameters to the measured material properties is described in Ref. [5, Chapter 9].

9.5 Healing Identification

For healing modeling, all that is required is experimental determination of the healing efficiency as a function of damage. Under shear loading G_{12}, the amount of damage d_1 in the fiber direction is negligible when compared to the amount of damage d_2 transverse to the fibers. Therefore, the change in the (unloading) shear modulus due to both damage and healing is given by

$$G_{12}^d = \overline{G}_{12}(1 - d_2 + h_2) \tag{9.22}$$

and the healing efficiency can be calculated as

$$\eta_2 = \frac{G_{12}^h - G_{12}^d}{\overline{G}_{12} - G_{12}^d} \tag{9.23}$$

Taking into account that the induced damage d_2 is a function of the applied strain, it is possible to represent the efficiency as a function of damage with a polynomial as follows:

$$\eta_2 = 1 + a\, d_2 + b\, d_2^2 \tag{9.24}$$

as shown in Figure 9.5.

Twenty-two unidirectional samples containing self-healing system were loaded in shear with one and one-half cycles consisting of loading, unloading, followed by 48 h of healing time, and reloading [3]. Each specimen was loaded to a unique value of maximum applied shear strain in the range 0.5–4.0% with roughly equal number of specimens loaded up to 0.5, 1.0, . . . , 4.0% at intervals of 0.5%. A yield strain threshold value of 0.43% was found for the specimens with self-healing system [3].

Recovery was measured for each level of strain and from it the healing is calculated using Equation 9.23. The tests used to characterize efficiency consist of two loading cycles separated by healing. For the particular situation of just one reloading after healing, such as in these tests, efficiency is a function of strain as well as damage. However, for the more general case of multiple loading cycles, the amount of damage is a more appropriate independent variable to define the efficiency function.

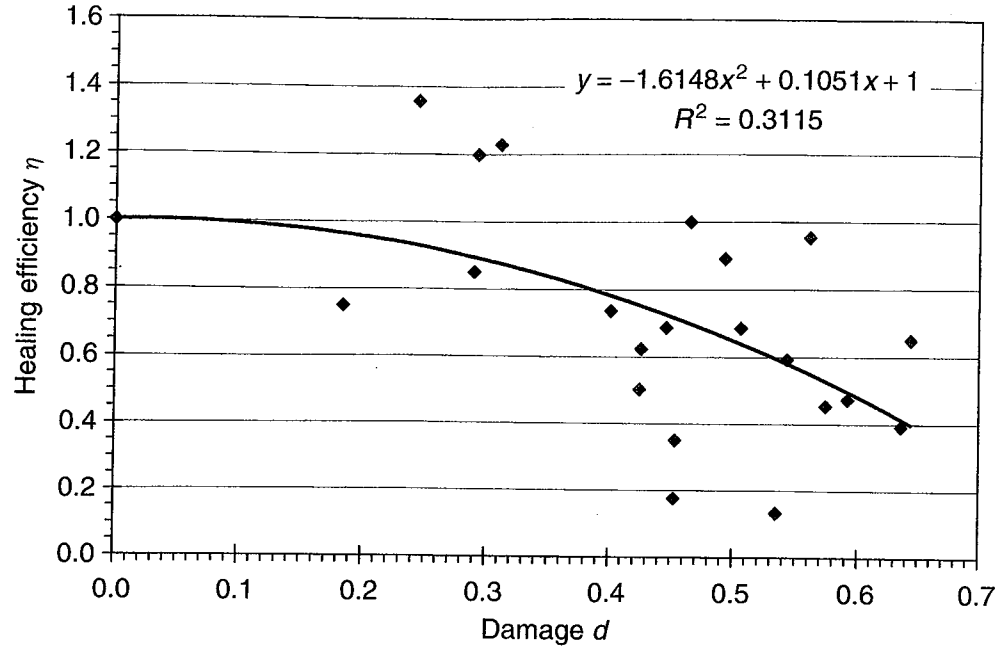

Fig. 9.5 Healing efficiency versus transverse damage.

Damage is a state variable; that is, damage describes univocally the state of accumulated damage regardless of the path followed to reach such damage. The total strain applied during multiple loading cycles is not a state variable because it can be achieved by various combinations of strain applied on each cycle. Each different combination would yield, in general, a different amount of damage. Therefore, even though applied strain is measured in the experiments, the amount of induced damage, not strain, is used to define the efficiency function. Shear tests are performed

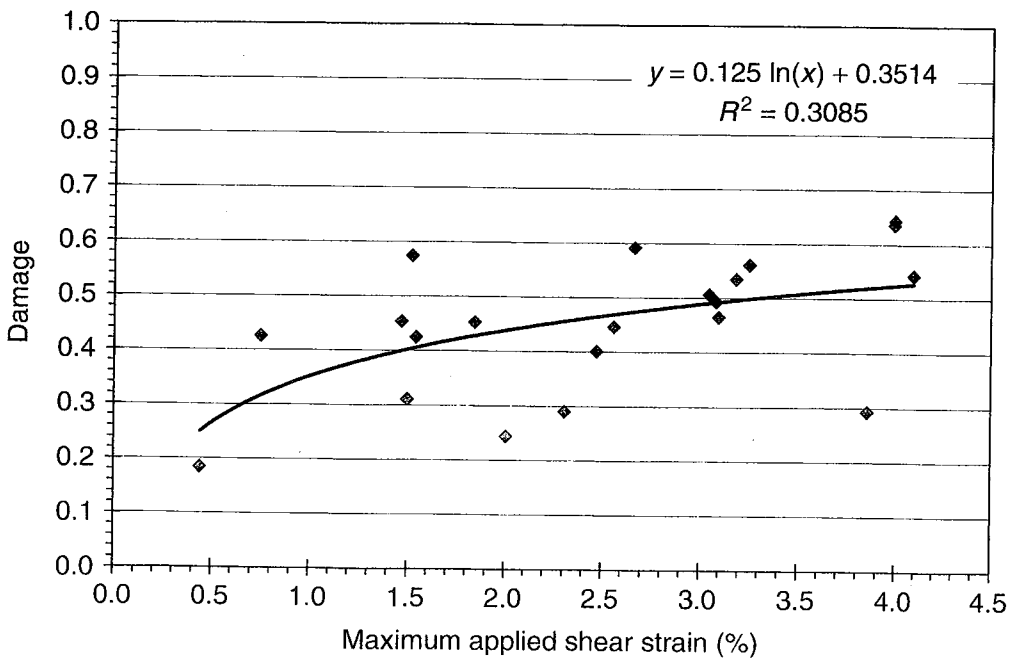

Fig. 9.6 Owing to hardening, increasingly large amounts of strain must be applied in order to produce more damage.

at strain levels of 0.25...4%. The healing efficiency from all specimens at each strain level (or damage level) are used to fit Equation 9.24, as shown in Figure 9.6.

9.6 Damage and Healing Hardening

Damage is represented by a state variable that accounts for the history of damage along the material principal directions (1, fiber-; 2, transverse-; 3, thickness direction). Once a certain level of damage is present, it takes higher stress (or strain) to produce additional damage (Figure 9.6). In this case, it is said that the material hardens. Damage hardening is represented by a hardening function, which is a function of the hardening variable δ. The effect of the hardening function is to enlarge the damage surface (Equation 9.12) that limits the stress space where damage does not occur. Damage hardening is represented in Figure 9.6 by a logarithmic function

$$d_2 = a' \ln(\gamma) + b' \tag{9.25}$$

as shown in Figure 9.5. It can be seen that additional strain must be applied in order to increase the amount of damage, thus hardening takes place.

Healing has two effects. First, it reverses some or all of the damage so that the stiffness of the material is recovered. At the same time, it resets the hardening threshold to a lower value, so that new damage can occur upon reloading at lower stress than would otherwise be necessary to cause additional damage on an unhealed material. This is merely a computational description of experimental observations. Such behavior can be interpreted as follows. The healed material can be damaged by reopening of the healed cracks, by creating new cracks, or by a combination thereof. In any case, the hardening function must be reset upon healing to be able to represent correctly the observed behavior.

In order to update hardening due to healing, first it is necessary to calculate how much of the damage can be healed. Since the self-healing system can only heal matrix damage, the damage that can be healed in the fiber direction is zero. The total damage that can be healed is then calculated as the sum of the damage in the two directions that can be healed

$$d^h = d_2 + d_3 \tag{9.26}$$

Next, the ratio of damage that can be healed in each direction to the total damage are calculated as

$$d_2^h = \frac{d_2}{d^h}; \quad d_3^h = \frac{d_3}{d^h} \tag{9.27}$$

By taking the healing efficiency into account, the amount of hardening recovered from healing in each direction can be calculated as

$$\mu_2 = \eta_2 \delta; \quad \mu_3 = \eta_3 \delta \tag{9.28}$$

Then, the overall hardening recovered from healing is calculated as

$$\mu = \mu_2 d_2^h + \mu_3 d_3^h \tag{9.29}$$

The amount of hardening recovered μ due to healing depends on the amount of healing that occurs in each direction. If the damage and healing phenomena are dominant in one direction, then that direction's healing efficiency will control the amount of recovery of hardening. Finally, the damage hardening parameter is updated as

$$\delta = \delta - \mu \tag{9.30}$$

9.7 Verification

The damage-healing model was identified using experimental data from a [0/90] symmetric as explained in Sections 9.4–9.6. Material properties are shown in Table 9.1.

ANSYS is compiled with a user subroutine implementing the damage-healing model. Finite element analysis is then used to represent the behavior of the sample materials. Model prediction and experimental data from a [0/90] specimen not used in the material characterization study and a quasi-isotropic $[0/90/45/-45]_S$ laminate are presented here for verification.

Shear tests of a single $[0/90]_S$ specimen was preformed. Quasi-static tests of the specimen loaded to 2.25% strain, unloaded, healed, and loaded again are shown in Figure 9.7. It can be seen that the computational model tracks the damaging Stress–strain behavior very well. Furthermore, the healing efficiency for this particular specimen was calculated using Equation 9.23 and used in the model. Comparison between experimental data and model prediction for the second (healed) loading of the specimen is shown also in Figure 9.7, where it can be seen

Table 9.1 Material properties of unidirectional composite.

Material property	Without self-healing	Standard deviation	With self-healing	Standard deviation
E_1 (MPa)	34 784	2185.89	30 571	4185
E_2 (MPa)	13 469	587.32	8699	829
υ_{12}	0.255	0.032	0.251	0.035
G_{12} (MPa)	3043	439.74	2547	207
F_{1t} (MPa)	592.3	29.32	397	66
F_{1c} (MPa)	459.1	43.66	232	59
F_{2t} (MPa)	68.86	9.17	45	10
F_{2c} (MPa)	109.5	9.25	109	9
F_6 (MPa)	49.87	3.39	38	2

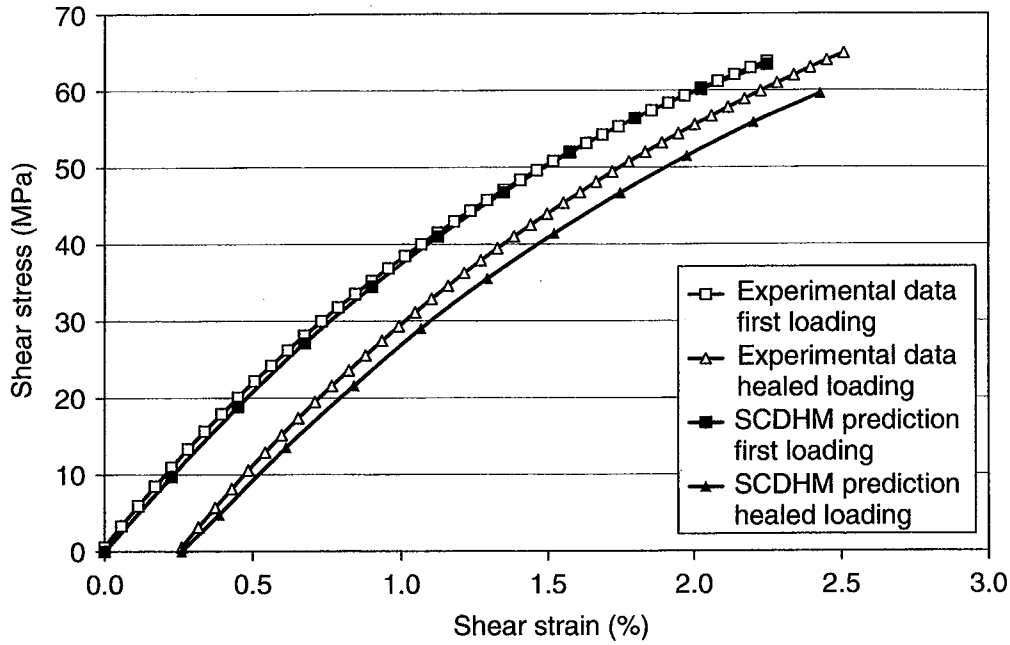

Fig. 9.7 Comparison between predicted response and experimental data for the first loading (damaging) and second loading (after healing) of a $[0/90]_S$ laminate.

that the computational model tracks reasonably well the damaging stress–strain behavior after healing.

Shear tests of a quasi-isotropic $[0/90/45/-45]_S$ laminate were preformed. Damage-healing tests of three specimens loaded to 1.5% strain and four specimens loaded to 2.25% strain were conducted. The loading shear stress–strain data of each specimen is then fitted with the following equation:

$$\sigma_6 = a'' + b'' \exp(-k''\gamma_6) \tag{9.31}$$

The parameters a'', b'', k'' of all the specimens loaded to the same strain level (say 2.25%) are then averaged. Comparison of model predictions with the first (damaging) loading up to 2.25% strain is shown in Figure 9.8. The damage model predicts the actual damaging behavior very well. This is notable because the model parameters were adjusted with an entirely different set of samples, which shows significant variability (see Table 9.1 and [3, Table 2]). Comparison of model predictions with the second loading (after healing) of the same set of four samples is shown in Figure 9.8. Again, the accuracy of the model is remarkable.

In summary, microcapsules were fabricated in the same manner outlined in the literature. Grubbs' first generation ruthenium catalyst was encapsulated in the same manner outlined in the literature. Fiber-reinforced laminates were fabricated with the self-healing system dispersed within the laminae. Tests were conducted to quantify the damage, plasticity, and healing parameters in the self-healing computational model. Additional tests on samples not used in the parameter identification were performed in order to verify the predictive capabilities of the

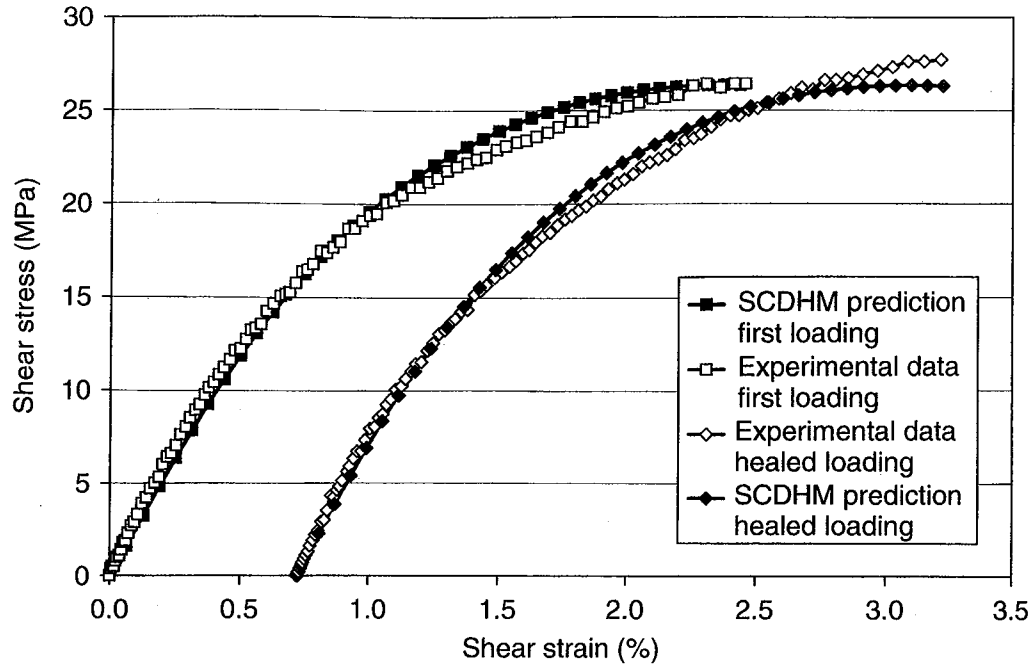

Fig. 9.8 Comparison between predicted response and experimental data for the first loading (damaging) and second loading (after healing) of a $[0/90/45/-45]_S$ laminate.

proposed model. It is observed that the proposed computational model tracks well the loss of stiffness due to damage, damage hardening, healing recovery, healing hardening, and damaging stress–strain behavior after healing.

References

1 Barbero, E.J. (**1999**) *Introduction to Composite Materials Design*. Taylor & Francis, Philadelphia, PA.

2 White, S., Sottos, N., Geubelle, P., Moore, J., Kessler, M., Sriram, S., Brown, E. and Viswanathan, S. (**2001**) "Autonomic healing of polymer composites". *Nature*, **409** 794–97. (Erratum *Nature*, **415** (6873), 817).

3 Barbero, E.J. and Ford, K.J. (**2007**) "Characterization of self-healing fiber-reinforced polymer-matrix composite with distributed damage". *Journal of Advanced Materials (SAMPE)*, **39** (4), 20–27

4 Barbero, E.J., Greco, F. and Lonetti, P. (**2005**) "Continuum damage-healing mechanics with application to self-healing composites". *International Journal of Damage Mechanics*, **14** (1), 51–81.

5 Barbero, E.J. (**2007**) *Finite Element Analysis of Composite Materials*, Taylor & Francis, Boca Raton, FL.

6 White, S., Sottos, N., Guebelle, P., Moore, J., Kessler, M., Sriram, S., Brown, E. and Viswanathan, S. (**2001**) "Autonomic healing of polymer composites". *Nature*, **409** (6822), 794–97.

7 Brown, E., Sottos, N. and White, S. (**2002**) "Fracture testing of a self-healing polymer composite". *Experimental Mechanics*, **42** (4), 372–79.

8 Kessler, M. and White, S. (**2001**) "Self-activated healing of delamination damage in woven composites". *Composites Part A Applied Science and Manufacturing*, **32** (5), 683–99.

9 Miao, S., Wang, M.L. and Schreyer, H.L. (**1995**) "Constitutive models for healing of materials with application to compaction of crushed

rock salt". *Journal of Engineering Mechanics*, **121** (10), 1122–29.

10 Jacobsen, S., Marchand, J. and Boisvert, L. (**1996**) "Effect of cracking and healing on chloride transport in opc concrete". *Cement and Concrete Research*, **26** (6), 869–81.

11 Jacobsen, S. and Sellevold, E.J. (**1996**) "Self healing of high strength concrete after deterioration by freeze/thaw". *Cement and Concrete Research*, **26** (1), 55–62.

12 Nakao, W., Mori, S., Nakamura, J., Takahashi, K., Ando, K. and Yokouchi, M. (**2006**) "Self-crack-healing behavior of mullite/sic particle/sic whisker multi-composites and potential use for ceramic springs". *Journal of the American Ceramic Society*, **89** (4), 1352–57.

13 Ando, K., Furusawa, K., Takahashi, K. and Sato, S. (**2005**) "Crack-healing ability of structural ceramics and a new methodology to guarantee the structural integrity using the ability and proof-test". *Journal of the European Ceramic Society*, **25** (5), 549–58.

14 Adam, J. (**2000**) A mathematical model of wound healing in bone, in *Proceedings of the International Conference on Mathematics and Engineering Techniques in Medicine and Biological Sciences*. METMBS'00, Vol. **1**, CSREA Press University of Georgia, Las Vegas, NV, pp. 97–103.

15 Adam, J. (**1999**) "A simplified model of wound healing (with particular reference to the critical size defect". *Mathematical and Computer Modelling*, **30** (5-6), 23–32.

16 Simpson, A., Gardner, T.N., Evans, M. and Kenwright, J. (**2000**) "Stiffness, strength and healing assessment in different bone fractures - a simple mathematical model". *Injury*, **31**, 777–81.

17 Lubliner, J. (**1990**) *Plasticity Theory*, Macmillan, Collier Macmillan, New York.

18 Schwartz, M.M. (**1997**) *Composite Materials: Properties, Non-Destructive Testing, and Repair*. Prentice Hall PTR, Upper Saddle River, NJ,Vol. **1**.

19 Wool, R. and O'Connor, K. (**1981**) "A theory of crack healing in polymers". *Journal of Applied Physics*, **52** (10), 5953–63.